



THIS MANUSCRIPT HAS BEEN SUBMITTED TO THE JOURNAL OF GLACIOLOGY AND HAS NOT BEEN PEER-REVIEWED.

The role of thermal notch erosion in forcing localised calving failure and short-term increases in velocity at a lake-terminating glacier in southeast Iceland

Journal:	<i>Journal of Glaciology</i>
Manuscript ID	JOG-23-0067.R2
Manuscript Type:	Article
Date Submitted by the Author:	n/a
Complete List of Authors:	Baurley, Nathaniel; University of Southampton, Department of Geography and Environmental Science Hart, Jane; University of Southampton, Department of Geography and Environmental Science
Keywords:	Glacier calving, Ice velocity, Remote sensing, Glacier monitoring, Mountain glaciers
Abstract:	We utilised repeat high-resolution UAV-SfM surveys, alongside terrestrial photography acquired in-situ, to investigate, for the first time, how localised calving failure can drive short-term increases in velocity at a lake-terminating glacier. This data was acquired over five days in early July 2019, and across 11 days in July 2021, to provide insights into a suite of processes that have been rarely studied. We demonstrate that large calving events (surface area $>1000 \text{ m}^2$, $>150 \text{ m}$ wide), occurring as a direct result of thermal notches at the waterline, can drive short-term increases in velocity up to 30% above the average, which are sustained for several days and occur over a much larger area of the glacier than was originally impacted by the initial calving event. We suggest that these findings present an important, yet previously undocumented aspect of the dynamic behaviour of both freshwater and tidewater glaciers, warranting further research into these key processes.



SCHOLARONE™
Manuscripts

1 **The role of thermal notch erosion in forcing localised calving**
2 **failure and short-term increases in velocity at a lake-terminating**
3 **glacier in southeast Iceland**

4 **Nathaniel R. Baurley^{1*} and Jane K. Hart¹**

5 ¹Geography and Environmental Science, University of Southampton, Southampton, United
6 Kingdom.

7 ***Correspondence:**

8 Nathaniel R. Baurley

9 n.baurley@soton.ac.uk

10 **Keywords: thermal notch erosion, glacier calving, glacier velocity, uncrewed aerial**
11 **vehicles, lake-terminating glaciers, glacier dynamics, structure from motion**
12 **photogrammetry, glacier monitoring.**

13 **ABSTRACT**

14 We utilised repeat high-resolution UAV-SfM surveys, alongside terrestrial photography
15 acquired in-situ, to investigate, for the first time, how localised calving failure can drive
16 short-term increases in velocity at a lake-terminating glacier. This data was acquired over five
17 days in early July 2019, and across 11 days in July 2021, to provide insights into a suite of
18 processes that have been rarely studied. We demonstrate that large calving events (surface
19 area >1000 m², >150 m wide), occurring as a direct result of thermal notches at the waterline,
20 can drive short-term increases in velocity up to 30% above the average, which are then
21 sustained for several days and occur over a much larger area of the glacier than was originally
22 impacted by the initial calving event. We suggest that these findings present an important, yet
23 previously undocumented aspect of the dynamic behaviour of both freshwater and tidewater
24 glaciers, warranting further research into these key processes.

25 **1. INTRODUCTION**

26 Frontal ablation, or the loss of ice from the termini of calving glaciers, occurs by a
27 combination of “mechanical” iceberg calving and subaqueous melt (Truffer and Motyka,
28 2016; How and others, 2019; Carrivick and others, 2020). Mechanical calving can occur via
29 four mechanisms: (i) longitudinal stretching; (ii) stresses associated with force imbalances at
30 the ice front; (iii) melt undercutting of the ice front; and (iv) torque arising from buoyant
31 forces (Benn and others, 2007). Subaqueous melt, meanwhile, in addition to melting the
32 terminus face directly, can further enhance mechanical calving by undercutting and
33 destabilising the subaerial portion of the glacier front (O’Leary and Christoffersen, 2013;
34 Luckman and others, 2015; How and others, 2019).

35 The process of subaqueous melt, and specifically melt undercutting, plays an important
36 role in controlling both the calving rate and overall stability of calving glaciers in both
37 freshwater and tidewater settings (Luckman and others, 2015; Truffer and Motyka, 2016;
38 Benn and Åström, 2018). Indeed, it is now recognised as a highly significant process,
39 particularly in those environments where relatively warm water is brought into contact with
40 glacier termini, including fjords in Alaska, Svalbard and Greenland, and lakes in Patagonia

41 and New Zealand (e.g., Dykes and others, 2011; Bartholomaeus and others, 2013; Rignot and
42 others, 2015; Minowa and others, 2017; Schild and others, 2018). In these settings, melt is a
43 function of the water temperature and the tangential movement of this water across the ice
44 front, which ensures efficient energy transfer (Jenkins and others, 2011; Pełlicki and others,
45 2015; Benn and Åström, 2018).

46 As such, whenever melt rates at the waterline exceed those above, the calving front will
47 be progressively undercut, leaving the subaerial portion of the terminus overhanging a sub-
48 horizontal waterline notch, resulting in an increase in force imbalance at these locations
49 (Röhl, 2006; Benn and others, 2007; Pełlicki and others, 2015). Calving can then occur along
50 preferential lines of weakness (e.g., surface crevasses), either as low magnitude events where
51 undercuts are small, resulting in localised, shallow subaerial failures, or as high magnitude
52 events where undercuts are large, resulting in the collapse of the entire ice column (Benn and
53 others, 2007; 2017; Mallalieu and others, 2020). For those glaciers where melt undercutting is
54 the primary control on calving, whether they calve via low or high magnitude events will
55 have important implications for the long-term calving rate, and consequently, the dynamic
56 behaviour and overall stability of these glaciers across different spatial and temporal scales
57 (O’Leary and Christoffersen, 2013; How and others, 2019).

58 Indeed, there is the potential that these high magnitude events could even drive short-
59 term variations in ice dynamics, with observations from several tidewater glaciers in
60 Greenland suggesting that particularly large calving events (which are not necessarily forced
61 by melt undercutting) can result in an acceleration of ice flow that is sustained long after the
62 initial event occurred (Nick and others, 2009; Howat and others, 2010; Murray and others,
63 2015). Yet although speed-ups in response to undercut-driven calving are yet to be observed
64 in nature, the potential for such events to occur raises important implications for the
65 dynamics and overall stability of these glaciers. However, while further work is required in
66 order to better understand these processes, most studies over recent years have predominately
67 been undertaken in tidewater environments, particularly in Svalbard and Greenland (e.g.,
68 Luckman and others, 2015; Rignot and others, 2015; Jouviet and others, 2018; Schild and
69 others, 2018).

70 In contrast, while melt undercutting and notch erosion have been known to be
71 important drivers of calving losses in freshwater environments for over two decades (e.g.,
72 Kirkbride and Warren, 1997; Haresign and Warren, 2005; Röhl, 2006), since this time the
73 number of studies has been severely limited (e.g., Mallalieu and others, 2017; Minowa and
74 others, 2017). Most recently, Mallalieu and others (2020) were able to provide the first
75 continuous year-round record of calving processes in a freshwater setting by using an
76 integrated time-lapse and structure from motion (SfM) approach, identifying two distinct
77 calving regimes which they relate to melt undercutting and variations in lake ice. In general,
78 however, a lack of quantitative data relating to calving processes and their associated drivers
79 means these processes are not well understood (Purdie and others, 2016; Mallalieu and
80 others, 2020). Furthermore, no study (to the best of our knowledge) has investigated the role
81 that undercut-driven calving may have in forcing short-term increases in velocity, specifically
82 for those glaciers in freshwater settings. As such, the relative importance of these processes in
83 forcing the dynamics and stability of freshwater calving glaciers remains difficult to assess.

84 Uncrewed aerial vehicles (UAVs) may provide new opportunities and insights,
85 however, due to their ability to offer rapid repeat assessments of glacier surface dynamics at
86 extremely high spatial (cm-scale) and temporal (sub-daily) resolutions (Whitehead and
87 others, 2013; Ryan and others, 2015; Chudley and others, 2019). Indeed, when combined

88 with modern and relatively low-cost SfM techniques, the method can be used to generate
89 detailed orthomosaics and DEMs of the ice surface and surrounding morphology, from which
90 a number of different glacier-specific products can be derived with relatively low error (e.g.,
91 Immerzeel and others, 2014; Wigmore and Mark, 2017; Bash and others, 2018; Yang and
92 others, 2020). The UAV-SfM approach has previously been used to investigate the velocity
93 of calving glaciers (e.g., Ryan and others, 2015; Jouvét and others, 2019) as well as their
94 calving dynamics (e.g., Jouvét and others, 2017, 2019), however, the influence of calving on
95 forcing short-term speed-up events, driven by melt-undercutting at the waterline, has yet to
96 be assessed using this method, providing scope for its deployment here.

97 Consequently, in this study we utilise repeat high-resolution UAV-SfM surveys,
98 alongside terrestrial photography acquired in-situ, to investigate the role of thermal notch
99 erosion in forcing localised calving failure and subsequent short-term increases in velocity at
100 an actively calving lake-terminating glacier in southeast Iceland. More specifically, we aim to
101 (i) quantify how thermal notches develop and evolve at the waterline over time; (ii) evaluate
102 the extent to which large calving events are controlled by these notches; and (iii) investigate
103 whether these large calving events drive short-term increases in velocity across different
104 spatial and temporal scales. The findings of this study present an important and previously
105 undocumented aspect of calving glacier behaviour, which has the potential to occur in both
106 freshwater and tidewater settings. Consequently, we suggest future work should investigate
107 the relative importance of these processes for other calving glaciers in similar settings, in
108 order to better understand their current dynamic behaviour and overall stability.

109 2. STUDY AREA

110 Fjallsjökull (64°01'N, 16°25'W) is a large lake-terminating glacier situated on the southern
111 side of the Vatnajökull Ice Cap, in southeast Iceland (Fig. 1) (Evans and Twigg, 2002; Dell
112 and others, 2019). The glacier has an area and length of ~44.6 km² and ~12.9 km,
113 respectively, and like many glaciers in Iceland has undergone significant recession over the
114 last century, particularly since the early 2000s (Hannesdóttir and others, 2015; Guðmundsson
115 and others, 2019). This ongoing retreat has led to the emergence of a substantial
116 overdeepening (~206 m deep, ~3 km wide and ~4 km long), resulting in the development of
117 the large proglacial lake Fjallsárlón (~3.7 km²) into which the glacier currently terminates
118 (Magnússon and others, 2012; Guðmundsson and others, 2019).

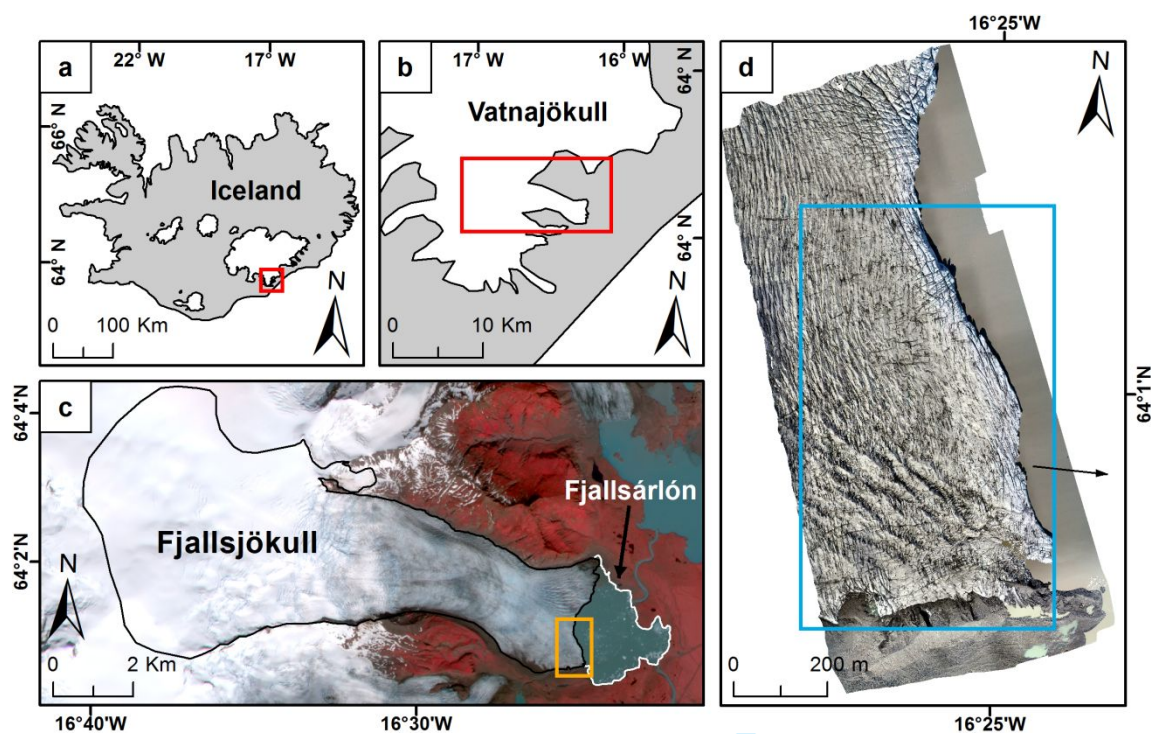
119 Recent research by Dell and others (2019) has indicated that the deep subglacial
120 topography and continued expansion of Fjallsárlón have become important controls for the
121 overall dynamics of the glacier, particularly over recent decades. The authors also suggest
122 that calving at Fjallsjökull likely occurs by a combination of buoyant forces acting on the
123 terminus, melt undercutting and force imbalances at terminal ice cliffs, particularly in those
124 locations where the bed topography is deepest, although they were unable to provide direct
125 evidence for any these processes occurring. As such, the role of melt undercutting (i.e.,
126 thermal notch erosion) as a control on calving activity and subsequent short-term velocity
127 increases remains poorly understood.

128 3. DATA AND METHODS

129 3.1. Repeat UAV-SfM Surveys

130 UAV-SfM surveys at Fjallsjökull were conducted over five days in early July 2019, and
131 across 11 days in July 2021. These surveys were undertaken using two different UAV

132 systems: a 3DR Solo quadcopter (2019) and a DJI Inspire 2 (2021). The technical
 133 specifications of both UAV systems, and the specific camera settings used, are given in
 134 Tables S1 and S2. For both years, all surveys were pre-designed using parallel flight lines
 135 placed orthogonal to ice flow direction, with full coverage of the study region obtained by
 136 undertaking multiple flights, ensuring sufficient inclusion of stable ground areas adjacent to
 137 the glacier terminus for use in the uncertainty assessment (Figs. S1a, S1b). All surveys were
 138 then flown autonomously at a constant elevation, resulting in a GSD of 0.03 m for both the
 139 2019 and 2021 surveys. Key flight parameters from both years are shown in Table 1, while
 140 specific details of each individual survey, including dates, number of flights and the number
 141 of photos captured, are given in Table S3.



142 **Fig. 1.** (a) Location of Fjallsjökull within Iceland, and (b) within the Vatnajökull Ice Cap. (c)
 143 Area of Fjallsjökull and Fjallsárlón as of July 2021. Glacier outline obtained from the GLIMS
 144 database, with the orange box depicting the areal extent of (d). Background is a 4-band false-
 145 colour PlanetScope acquisition from 7 July 2021. (d) UAV-SfM orthomosaic from 7 July
 146 2021, with the blue box illustrating the areal extent over which the analyses presented in this
 147 study are focused. Black arrow indicates the average ice flow direction in this region.
 148

149 To accurately georeference the 2019 imagery, a set of ground control points (GCPs)
 150 were deployed across stable ground near the lateral margin of the glacier, ensuring good
 151 spread in the X, Y and Z planes (Fig. S1c). The GCPs used here were high contrast, thick
 152 plastic markers, 1x1 m in size, with a clearly defined centroid to aid in locating the target
 153 centre during processing (Fig. S1d), with the centre position of each GCP recorded in the
 154 field using a Leica GS09 dGPS with an accuracy of <0.01 m. Seven GCPs were originally
 155 deployed around the study site at the start of fieldwork on 5 July 2019, although this was then
 156 increased to nine markers two days later.

157

158

159 **Table 1.** Flight parameters when undertaking the 2019 and 2021 UAV-SfM surveys.

160	Flight Parameters	2019	2021
161	Areal coverage (km ²)	0.511	0.858
162	UAV flying height AGL (m)	80	90
163	UAV flying speed (m s ⁻¹)	5.0	7.5
164	Image Overlap	90%	80%
165	Image Sidelap	70%	70%
166	GSD (m)	0.03	0.03

167 In contrast, due to the on-board differential carrier-phase GNSS functionality of the DJI
 168 Inspire 2, the 2021 imagery were instead accurately georeferenced using a PPK method after
 169 Tomsett and Leyland (2021) and Baurley and others (2022). This resulted in post-processed
 170 camera locations accurate to <0.05 m. However, a small network of ten GCPs were still
 171 deployed across the study site for redundancy (Fig. S1e). These were the same markers used
 172 in 2019, with the centre position of each GCP recorded using a Leica GS15 dGPS to <0.01
 173 m. Although it was intended that all UAV-SfM imagery from 2021 would be processed using
 174 the PPK method, a technical problem on 15 July meant no positional or timestamp data were
 175 recorded, and as such the images acquired from this day were georeferenced using the GCPs.

176 3.2. 3D Model Generation (SfM Photogrammetry)

177 All images from each survey were processed using an SfM workflow (e.g., Westoby and
 178 others, 2012) in Agisoft Metashape Professional v. 1.7 (Agisoft LLC, 2021). First, each
 179 image set was imported into Metashape, along with the relevant GCP and camera locations.
 180 An alignment procedure was then undertaken, based off the positional information of either
 181 the GCP locations (2019), or the post-processed camera locations (2021), resulting in
 182 georeferenced sparse point clouds. The only exception was for those surveys undertaken on 15
 183 July 2021, where the alignment procedure was undertaken using the GCP locations recorded
 184 in the field. Following this, an optimisation procedure was performed in order to remove non-
 185 linear deformations and georeferencing errors from the final models (Agisoft LLC, 2021).
 186 Dense point clouds were then generated, from which DEMs and orthomosaics for each
 187 survey day were produced, with these exported from Metashape at resolutions of 0.07 and
 188 0.03 m (2019), and 0.05 and 0.03 m (2021), respectively, for further analysis.

189 3.3. Uncertainty Assessment

190 The relative uncertainty of the generated 3D models from both 2019 and 2021 were assessed
 191 by undertaking a repeat assessment of stable ground topography, following the method of
 192 Tomsett and Leyland (2021) and Baurley and others (2022). This follows the principle that
 193 stable ground should be consistent between surveys and, therefore, any variations are
 194 indicative of the uncertainty in the system (e.g., Chudley and others, 2019; Yang and others,
 195 2020). This in turn affects the level of confidence in the data and the level of change that can
 196 be detected. Indeed, because an extensive ground control network could not be deployed in
 197 either 2019 or 2021 due to the relative inaccessibility of the glacier surface, this stable ground
 198 assessment was essential to identify any errors between the generated 3D models.

199 For this assessment, an area of ice-free stable ground near the lateral margin of the
200 glacier was selected that encompassed both shallow and steep topography and which was
201 present in all the generated dense point clouds. This region was then extracted from each
202 individual point cloud simultaneously to avoid any potential differences in stable ground
203 extent. Once selected, each point cloud was differenced to each of the others in a pairwise
204 fashion within CloudCompare v. 2.11.3, using the M3C2 algorithm developed by Lague and
205 others (2013). This allowed the error to be assessed by comparing the median error, the
206 Normalised Median Absolute Deviation (NMAD), as well as visualising their distribution, as
207 outlined by Höhle and Höhle (2009). These errors could then be used to identify the
208 minimum change detection threshold between surveys, which ensured that any differences
209 present in the point clouds (and thus resultant DEMs and orthomosaics) represented actual
210 change.

211 3.4. Thermal Notch Formation and Evolution

212 To investigate the presence and evolution of thermal notches across our study region, repeat
213 digital photographs of the calving front were acquired daily in both 2019 and 2021 using a
214 Nikon D3300 DSLR camera. Where possible, images were captured from the same location
215 (by using stone markers in the field) and at the same time of day (11:00) to ensure the
216 captured scene did not vary significantly between the different days. Note this location was
217 different in 2019 and 2021 due to recession of the ice margin. No image was captured on the
218 5 July 2019 due to a technical issue with the camera, so the image acquired on the 4 July was
219 used in subsequent analyses. Each image was then categorised into five notch types (Table
220 S4, Fig. S2):

- 221 (i) Stepped: Multiple notches which reverse back towards lake.
- 222
- 223 (ii) Extensive: Approx. >2 m deep, >1 day old.
- 224
- 225 (iii) Small: Approx. <2 m deep, >1 day old.
- 226
- 227 (iv) New: ~1 day old, approx. <0.5 m deep.
- 228
- 229 (v) Absent: Not present at waterline.

230 These were then used to create a rigorous time-series of notch formation and evolution. Note
231 some images were categorised into more than one type (e.g., stepped and extensive), whilst
232 the approximate notch vertical depth was estimated from the UAV-derived DEMs.

233 3.5. Variations in Frontal Position and Calving Events

234 To assess changes in calving front geometry and evolution, the position of the terminus in
235 each orthomosaic was manually digitised in ArcGIS using a fixed zoom scale of 1:30
236 throughout the entire digitisation process. To estimate the location and area of ice that calved
237 between two repeat flights, DEM differentiation was utilised, whereby the earlier DEM was
238 subtracted from the latter DEM to retrieve a spatially distributed map of change. The location
239 and area of each individual calving event was then manually digitised in ArcGIS, with the
240 corresponding differenced DEM used to define the horizontal extent of each event. The
241 uncertainty in both approaches was quantified through repeat digitisation techniques (at a
242 fixed zoom scale of 1:30), before calculating the standard error for each period (after Baurley
243 and others, 2020).

244 3.6. Localised Velocity Variations

245 To derive high-resolution velocity fields, the free software CIAS was utilised
246 (<https://www.mn.uio.no/geo/english/research/projects/icemass/cias/>), which allows glacier
247 surface displacements to be calculated with sub-pixel accuracy (Haug and others, 2010; Heid
248 and Käab, 2012). Prior to processing, each orthomosaic was first resampled to a resolution of
249 0.25 m, before georeferencing each orthomosaic pair in ArcGIS. Depending on the temporal
250 separation between successive orthomosaics, the specific processing parameters varied, with
251 these given in Table S5. The resulting displacements were then filtered by direction and
252 magnitude, following a similar approach to Robson and others (2018), before being
253 interpolated using ordinary kriging to produce velocity fields for each period.

254 To determine the uncertainty of these calculations, displacements were measured over
255 areas of stable ground that contained variable surface topography (Fig. S3) (e.g., Chudley and
256 others, 2019; Jouvét and others, 2019). This analysis was undertaken over three distinct zones
257 close to the glacier margin that were covered by both the 2019 and 2021 surveys, before
258 calculating the combined stochastic standard deviation. Stable ground locations were chosen
259 as theoretically no change should have occurred in these locations, and as such, they provide
260 a good estimation for the accuracy of the velocity calculations.

261 4. RESULTS

262 4.1. Uncertainty Assessment

263 The results of the stable ground assessment importantly display similar levels of consistency
264 between the different surveys from both 2019 and 2021. For the July 2019 comparisons (Fig.
265 S4), the median error between points was between -0.045 and 0.069 m (1.5-2.3 GSD), with
266 NMAD values no greater than ± 0.227 and as low as ± 0.097 m. Similarly, for the July 2021
267 comparisons (Fig. S5) the median error was between 0.04 and -0.099 m (~ 1.3 -3.3 GSD), with
268 NMAD values of between ± 0.04 and ± 0.26 m. As a result, these errors indicate that in both
269 years the difference between stable ground locations were small.

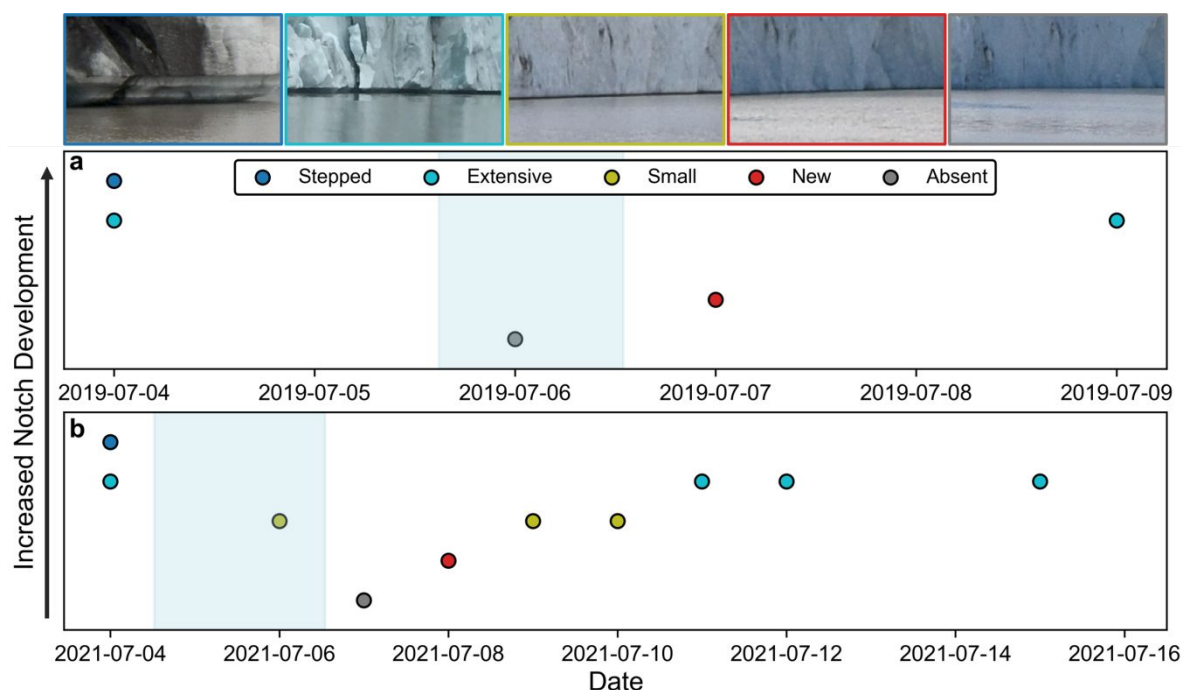
270 These errors also show very good agreement with those previous studies within glaciology
271 that have undertaken their own UAV-SfM surveys at similar flying heights to those
272 undertaken here. Across these studies, the range of reported errors was between 1.5 and ~ 3
273 times the GSD, with the flying heights of each respective survey ranging between 90 m and
274 110 m (e.g., Ely and others, 2017; Wigmore and Mark, 2017; Bash and others, 2018; Rossini
275 and others, 2018; Xue and others, 2021). Overall, the results of the uncertainty assessment
276 indicate that the errors found for all surveys across both years are smaller than the change
277 expected over each period of interest (decimetre-metre scale) and are thus well within the
278 realm of acceptability.

279 4.2. Thermal Notch Formation and Evolution

280 Our time series of notch formation and evolution (Fig. 2), as well as the complete set of
281 images acquired in both years (Figs. S6, S7), clearly indicates the presence of thermal
282 notches in this region of Fjallsjökull. In general, the notches are more extensive (both
283 vertically and horizontally) at the beginning of each study period, with their morphology
284 showing a clear stepped pattern which reverses back towards the lake. This is particularly
285 noticeable at the beginning of fieldwork in 2019 and may indicate that the level of the lake
286 dropped since the notches were first formed in order for the stepped pattern to be visible (Fig.

287 S6). In contrast, by the end of the study period these notches are morphologically less
 288 distinct, showing no stepped pattern, and with only a small reverse slope visible at the end of
 289 fieldwork in 2019, not in 2021.

290 Furthermore, our data also reveal distinct daily variations in the relative extent of these
 291 thermal notches, particularly for those observed in 2021 (Figs 2b, S7). For example, between
 292 the 4 and 7 July, the notches become steadily less extensive, so that by the 7 July no notches
 293 are visible in this region of the calving front. However, over the following few days a new set
 294 of notches can be observed forming at the waterline, and as a result by the end of the study
 295 period relatively extensive thermal notches are once again present, with a similar pattern also
 296 observed in the 2019 time series. Such a pattern likely reflects the occurrence of large calving
 297 events in this region, which have the effect of removing the notched portion of the terminus,
 298 causing the process of notch formation to reset.



299

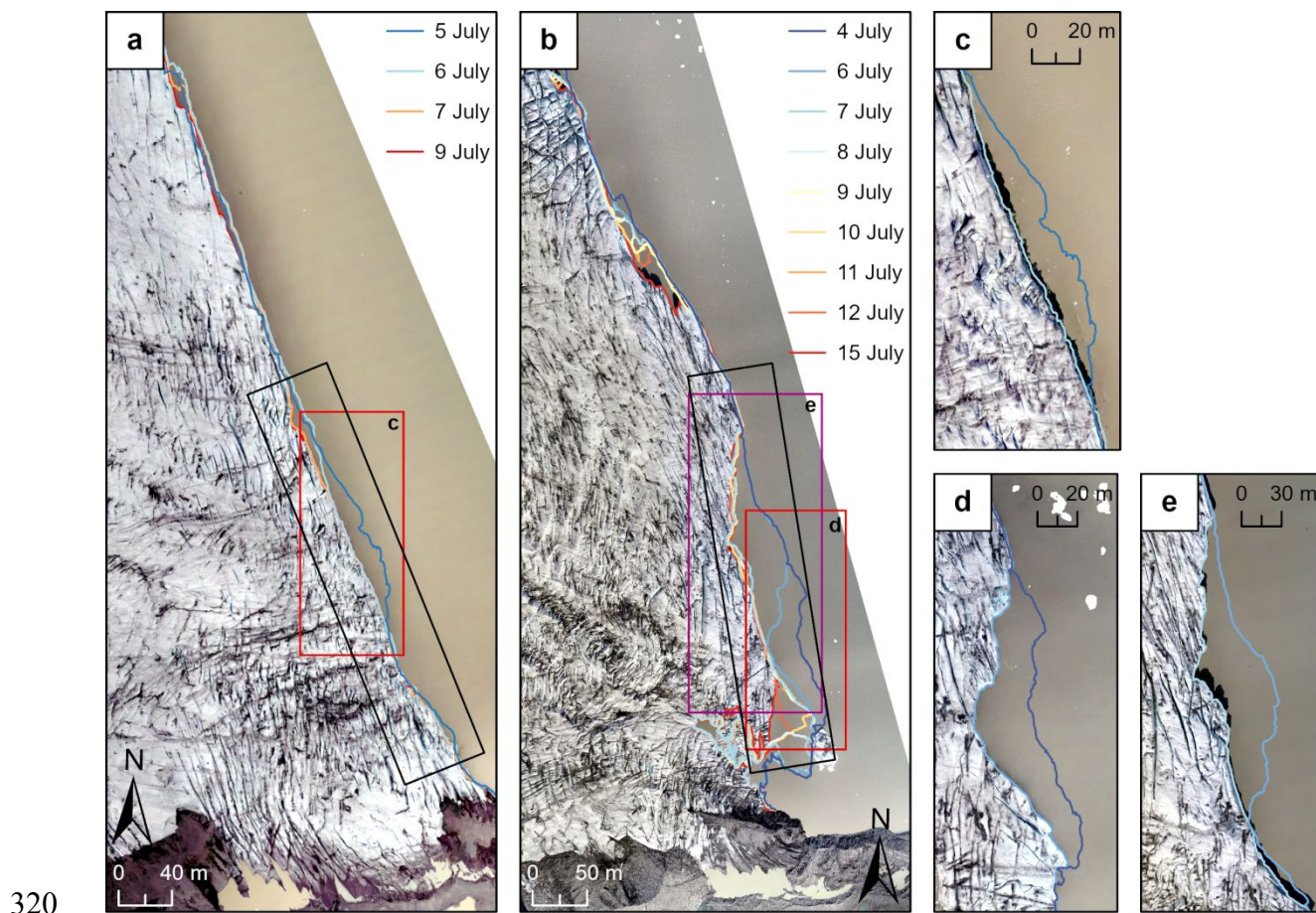
300 **Fig. 2.** Time series plot of notch evolution through time for (a) 2019 and (b) 2021, based on
 301 the repeat terrestrial photographs captured in the field. Each coloured point represents one of
 302 five notch types observed in this study. Example images of the five notch types are shown
 303 above (a) for reference. Blue shaded regions mark the period in which the large calving
 304 events (Section 4.3) are known to have occurred.

305 It is important to note that although no direct measurements of notch erosion could be
 306 made here, the fact they are present in nearly every photo, and in some cases very extensive,
 307 suggests the rates of notch erosion must be significant. Indeed, by using the produced DEMs
 308 we are able to estimate that the calving front in this region is ~25 m (2019) and ~20 m (2021)
 309 high, which based on the time series of imagery suggests that notches reaching up to at least
 310 ~2 m in vertical extent are not inconceivable.

311 4.3. Variations in Frontal Position and Calving Events

312 In general, the position of the calving front remained relatively stable across all time periods
 313 in both 2019 and 2021, with only a small number of significant changes in calving front
 314 geometry (i.e., large calving events) occurring during this time (Fig. 3). Indeed, in both years

315 calving is dominated by a high number of small events ($<100 \text{ m}^2$) (Table S6), with an average
 316 size of 55.63 m^2 and 233.06 m^2 in 2019 and 2021, respectively. As a result, the greatest
 317 changes in frontal position occur as a direct result of only three large calving events: one in
 318 2019, and two in 2021 (Figs. 3c-e). These events have a surface area of $>1000 \text{ m}^2$, and are
 319 $>150 \text{ m}$ wide.



320
 321 **Fig. 3.** Change in calving front position between (a) 5-9 July 2019 and (b) 4-15 July 2021.
 322 The lettered boxes in (a) and (b) indicate where the large calving events occurred in both
 323 years, with these presented in panels (c)-(e). The corresponding dates for these events are: (c)
 324 5-6 July 2019, (d) 4-6 July 2021, and (e) 6-7 July 2021. See main text for more detail on each
 325 individual event. Black boxes in (a) and (b) indicate the broad locations of the thermal
 326 notches observed in each year. Background in each panel is the orthomosaic for the latest
 327 period.

328 The 2019 large calving event occurred in the lower portion of the study region between
 329 the 5 and 6 July, in the exact same region as the observed thermal notches (Fig. 3a). The
 330 event was approximately 150 m by 20 m (at its widest point) and resulted in $\sim 1,579 \text{ m}^2$ of ice
 331 being lost, which is ~ 28 times larger than the average for this period. Similarly, the two large
 332 calving events that were observed in 2021 also occurred in the lower portion of the study
 333 region, with these again located in the same region as the observed thermal notches (Fig. 3b).
 334 The first of these events occurred between the 4 and 6 July, was approximately 155 m by 30
 335 m (at its widest point) and resulted in $\sim 2,948 \text{ m}^2$ of ice being lost, which is ~ 12 times larger
 336 than the average for this period. The second event occurred between the 6 and 7, in the exact
 337 same region as the first, but over a much greater extent, being approximately 200 m by $\sim 55 \text{ m}$
 338 (at its widest point). This resulted in $\sim 4,629 \text{ m}^2$ of ice being lost, which is ~ 1.5 times larger

339 than the first event, and ~ 20 times greater than the average for this period. Importantly, while
340 these large events are infrequent, only representing ~ 1 - 2% of the total calving events in 2019
341 and 2021, they account for $\sim 40\%$ of the total area lost through calving across both years,
342 illustrating the relative importance of these singular large events on calving losses overall.

343 It is important to note that the calculated standard error for both sets of analyses was
344 $< 1\%$ for all time periods in both years, indicating that the calculated uncertainty was not
345 greater than the change observed during this time.

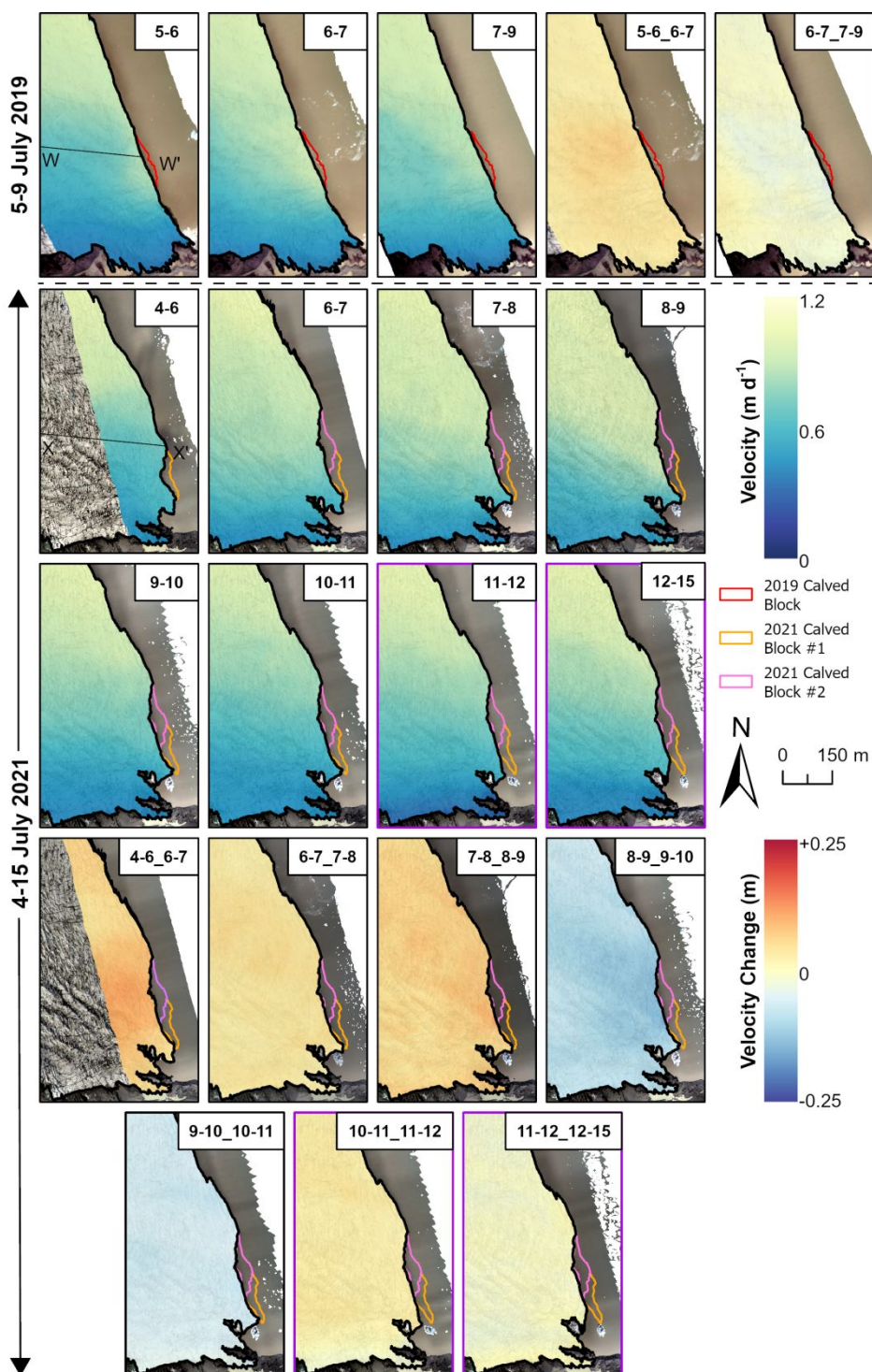
346 4.4. Localised Velocity Variations

347 The velocity results (Fig. 4) demonstrate an overall pattern, whereby velocities increase with
348 increasing distance from the southern-grounded margin, which is related to the influence of
349 the underlying bedrock topography (Baurley, 2022). Within this overall pattern, however,
350 smaller-scale, more localised velocity variations, which occur over several days, can also be
351 observed. For example, localised increases in velocity (i.e., speed-up events) occur between
352 both the 5 and 9 July 2019, and the 4 and 11 July 2021. These variations are clearly visible in
353 the velocity change rasters and seem closely related to the occurrence of the large calving
354 events described previously. Therefore, to further assess the influence of these events on the
355 ice velocity, for each period flow transects (shown in Fig. 4) were extracted from the middle
356 of where each calving event occurred back into the ice interior. These results are shown in
357 Fig. 5.

358 The 2019 speed-up event was initially limited to the region immediately surrounding
359 where the large calving event occurred, with velocities reaching a peak of $\sim 0.84 \text{ m d}^{-1}$ by the
360 6 July, which is $\sim 20\%$ faster than the average. A further increase in velocity was observed
361 over the following 24-hour period, reaching an event peak of $\sim 0.88 \text{ m d}^{-1}$ ($\sim 5\%$ faster than
362 the previous 24 hours), while the areal extent of this region of elevated velocities also
363 increased in this period. By the 9 July, despite peak velocities decreasing slightly to $\sim 0.86 \text{ m}$
364 d^{-1} , much of the region behind the calving front and into the glacier interior was still flowing
365 at elevated velocities, $\sim 12\%$ faster than at the onset of the speed-up event.

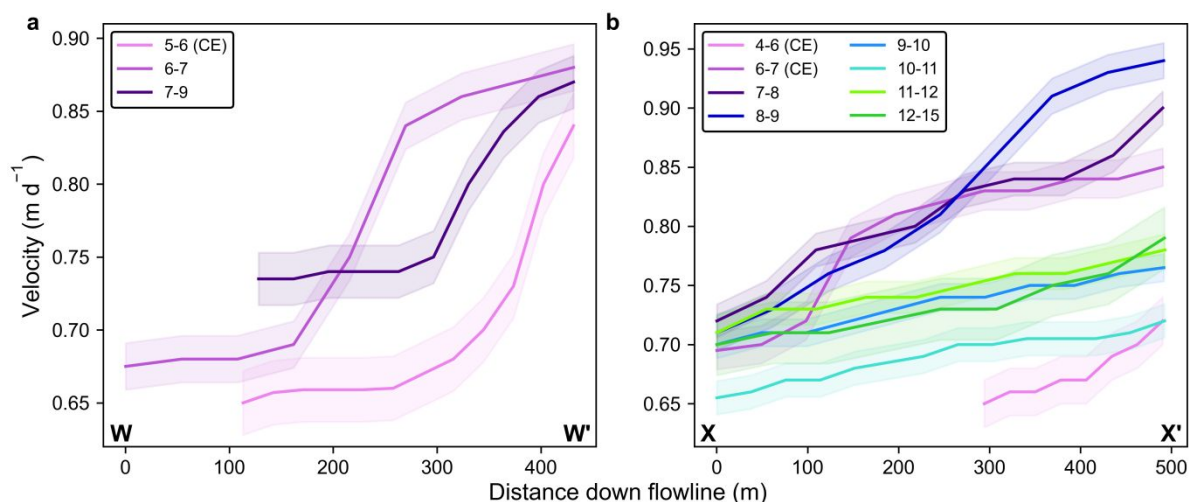
366 The 2021 speed-up event, like in 2019, was initially only limited to the region
367 surrounding where the first large calving event occurred, with velocities peaking at $\sim 0.72 \text{ m}$
368 d^{-1} by the 6 July, which is 15% faster than the average. In contrast to 2019, however,
369 following the occurrence of the second large calving event between the 6 and 7 July,
370 velocities continued to increase over the following 48 hours, only reaching the event peak of
371 $\sim 0.94 \text{ m d}^{-1}$ by the 9 July. This is $\sim 30\%$ faster than the velocity observed at the onset of the
372 event. Furthermore, the areal extent of this region of elevated velocities also increased in this
373 period, again reaching its maximum by the 9 July. After this point, however, velocities begin
374 to decrease, so that by the 11 July they have returned to a similar distribution and magnitude
375 as was observed \sim five days earlier, marking the cessation of the speed-up event.

376 Interestingly, there is a small ($\sim 0.05 \text{ m d}^{-1}$), additional increase in velocity observed
377 over the following 24 hours, which is maintained up to the 15 July (Fig. 5). This increase in
378 velocity is likely a result of several smaller calving events which also occurred in this region
379 during this time, although it is important to note that the overall influence of these events was
380 small compared to the large calving events and resultant speed-ups described previously.



381

382 **Fig. 4.** Horizontal velocity fields and velocity change rasters (sequential and diverging colour
 383 ramp, respectively) for all time periods, calculated using feature tracking on UAV-derived
 384 orthomosaics. Lines W-W' and X-X' denote the beginning and end, respectively, of the
 385 flowlines used to extract the velocity profiles presented in Fig. 5. Figure panels outlined in
 386 black correspond to those dates which were encompassed by the 2019 and 2021 speed-up
 387 events (described in detail in-text), whilst those outlined in pink reflect those dates in 2021
 388 where a small, additional increase in velocity was observed, which occurred in the days after
 389 the “main” speed-up event had ended. Location and size of the three large calving events
 390 are also shown. Average ice flow direction in this region is shown in Fig. 1d. Background in each
 391 panel is the orthomosaic for the latter period.



392

393 **Fig. 5.** Velocity profiles for all time periods in (a) 2019 and (b) 2021, generated by extracting
 394 the flowlines W-W' and X-X' from the relevant UAV-derived velocity fields shown in Fig. 4.
 395 Associated uncertainty margins for each period are also shown. "CE" refers to those time
 396 periods where the large calving events are known to have occurred.

397 Based on these observations from the 2021 speed-up event, we suggest a similar pattern
 398 also occurred during the 2019 event, whereby velocities would have returned to their pre-
 399 event magnitude in the days following the 9 July, despite no UAV surveys being undertaken
 400 after this date.

401 It is also important to note that during these speed-up events, the region of elevated
 402 velocities extended some several hundred metres back into the interior of the glacier,
 403 encompassing a much larger area than was originally influenced by the initial calving events,
 404 with these regions of elevated velocities also sustained for several days after these events
 405 occurred (Figs. 4, 5).

406 To further explore the relationship between the large calving events described in
 407 Section 4.3 and the speed-up events observed here, we extracted additional velocity transects
 408 from all rasters from both years, spaced at 100 m intervals along the entire ice front (which
 409 were covered by the respective UAV surveys, Figs. S8h, S9I). This analysis illustrates that in
 410 both years, away from the 300-400 m region impacted by the calving-induced speed-up
 411 events described above, there is little variation in the velocity between days, with no notable
 412 speed-up events observed (Figs. S8, S9). This suggests that the speed-up events described
 413 above only occurred as a result of the large calving events, providing further confidence in
 414 the validity of our findings.

415 Finally, following the stable ground accuracy assessment, the combined stochastic
 416 standard deviation for this analysis was $\pm 0.02 \text{ m d}^{-1}$ in both 2019 and 2021, which represents
 417 $\sim 2\text{-}3\%$ of the total ice motion in both years.

418 5. DISCUSSION

419 5.1. Formation and Evolution of Thermal Notches at Fjallsjökull

420 Thermal erosion notches have previously been reported at other lake-terminating glaciers in
 421 several regions, including New Zealand (e.g., Röhl, 2006; Dykes and others, 2011),
 422 Patagonia (e.g., Haresign and Warren, 2005; Minowa and others, 2017) and Greenland (e.g.,

423 Mallalieu and others, 2020). In these settings, notch formation is often controlled by a
424 combination of several factors, including water temperature, wind-driven wave action, ice
425 cliff geometry and water-level fluctuations (e.g., Röhl, 2006; Truffer and Motyka, 2016;
426 Minowa and others, 2017). Of these factors, it is how much the level of the water body
427 fluctuates that is often considered a key driver of notch formation in freshwater environments
428 (Benn and others, 2007; Mallalieu and others, 2020).

429 At Fjallsjökull, thermal notch formation is likely driven by a combination of relatively
430 warm surface water and variations in water-level, with the largest, most extensive notches
431 forming when the water-level remains relatively constant. This allows the heat energy from
432 the surface water to be concentrated in a narrower band of ice, promoting efficient notch
433 development (Röhl, 2006). Indeed, because the observed notches in both 2019 and 2021 were
434 extensive, particularly in depth (Figs. 2, S6 & S7), suggests that the level of Fjallsárlón must
435 have remained relatively consistent across both periods in order for these notches to form.
436 Furthermore, additional evidence is provided in both years through the time series of notch
437 evolution (Fig. 2), as well as the repeat terrestrial photographs of the calving front, which
438 have allowed the formation and growth of new thermal notches to be directly observed.

439 For example, in 2021, although notch formation had been reset following two large
440 calving events between the 4 and 7 July, less than 24 hours later, small notches could once
441 again be observed at the waterline, with these continuing to grow and develop over the
442 following four days (Fig. S7). As a result, by the 12 July these notches were once again as
443 extensive (both in size, as well as in area covered) as those first observed on the 4 July,
444 before the large calving events had occurred. A similar pattern of notch re-formation and
445 growth following calving was also observed in July 2019 (Fig. S6). These observations are
446 important, not only because they confirm that notch erosion is actively occurring, but also
447 because they indicate that the *rate* of notch erosion must be significant to allow these features
448 to form and grow at the waterline of Fjallsjökull in such a short period of time.

449 Although no direct measurements of notch erosion could be made here, the fact these
450 notches formed and evolved so rapidly means it is not inconceivable that rates of $\sim 0.5 \text{ m d}^{-1}$
451 may have been occurring in this region of Fjallsjökull in both years, similar to observations
452 made in previous studies (e.g., Minowa and others, 2017; Mallalieu and others, 2020). Such
453 rates could only have occurred, however, if the water level of Fjallsárlón remained relatively
454 consistent across each period. Unfortunately, no physical measurements of lake level could
455 be obtained in this study either, but direct observations made in the field (Figs. S6, S7)
456 indicates that the level of the lake fluctuated very little during either period, which would
457 have allowed such rates of notch erosion to occur. To our knowledge, this is one of the first
458 studies to directly observe the formation and growth of new thermal notches at the waterline
459 of a lake-terminating glacier following the occurrence of large calving events. As a result,
460 these observations may be important for our understanding of the role of thermal notches in
461 driving localised calving failure at Fjallsjökull.

462 **5.2. Calving Failure and Localised Speed-ups**

463 Thermal notches are integral to the calving process because they can undercut the terminus at
464 the waterline, increasing the force imbalance in these localities and thus promoting calving
465 failure (Benn and others, 2007; Mallalieu and others, 2020). As mentioned previously, three
466 large calving events were observed in this study (one in 2019, two in 2021), with all three
467 events occurring in the same part of the lower study region. Importantly, extensive thermal
468 notches were observed at the waterline on both the 4 July 2019, and the 4 and 6 July 2021,

469 within the same region where each of the three large calving events later occurred, strongly
470 suggesting that these notches were the primary driver behind each event (Figs 3a, 3b).

471 It is possible that these events may have also been driven by buoyant forces acting on
472 the terminus, which can be a relatively common driver of calving in freshwater environments
473 (e.g., Boyce and others, 2007; Dykes and others, 2011). To investigate this, we used our
474 UAV-derived DEMs to detect the presence or absence of terminus buoyancy across our study
475 region. Importantly, we find no clear evidence of these forces in the vicinity of the calving
476 front either directly before or after these large calving events occurred. Indeed, in the days
477 prior to calving the ice surface was very similar to, or indeed slightly lower than, the ice
478 surface in the days immediately after calving i.e., the ice surface elevation increased (slightly)
479 after calving. This indicates that inflexion and upward rotation of the ice surface prior to
480 calving, like observed by Murray and others (2015), was unlikely to be the primary cause of the
481 observed calving events. As such, we will now focus on the mechanisms by which notch
482 erosion caused these events to occur.

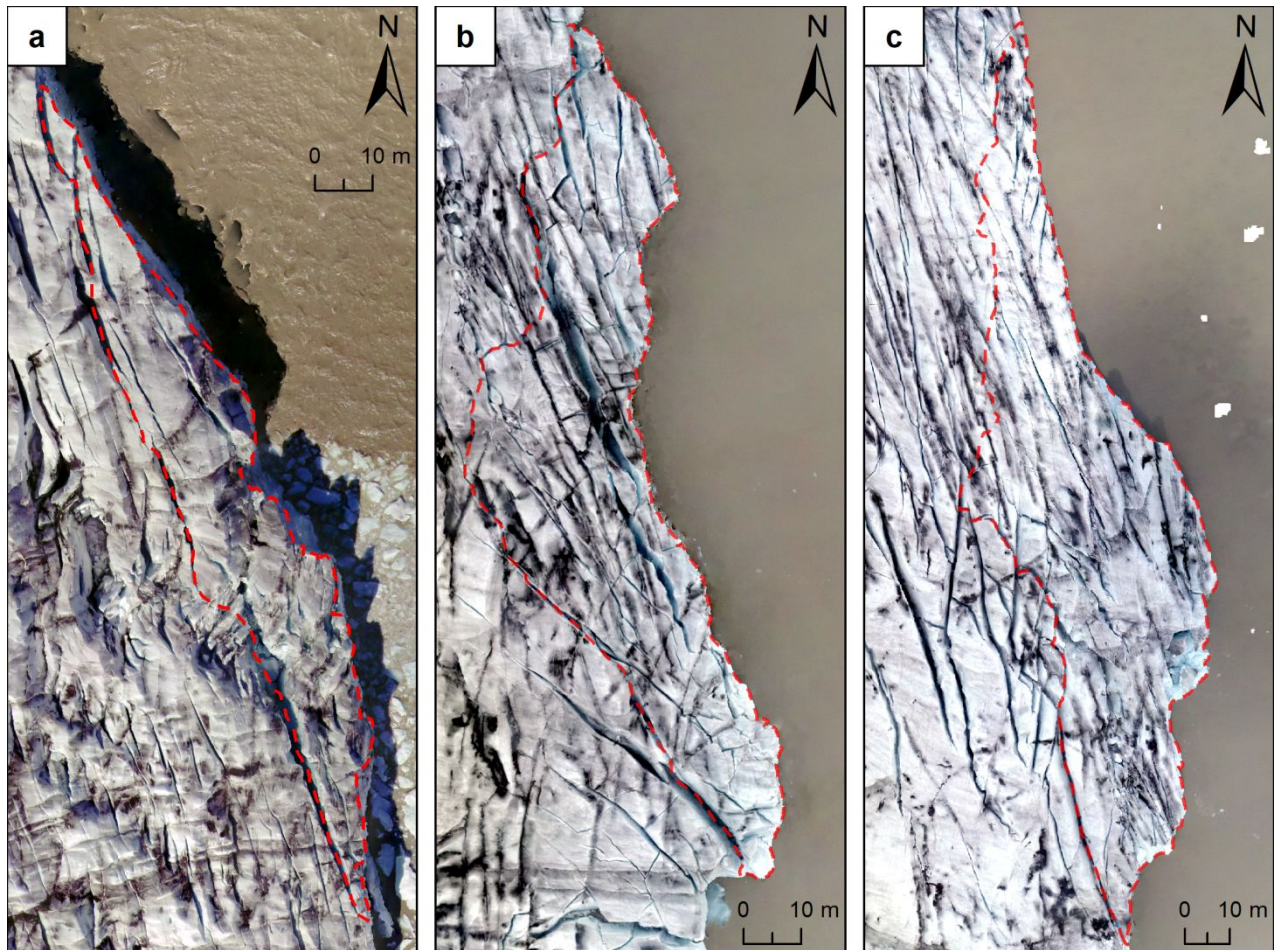
483 It was illustrated by Benn and others (2017) through discrete element modelling that
484 thermal notch undercutting can be associated with two types of calving failure: (i) low
485 magnitude events that occur where loss of support by undercutting exacerbates existing faults
486 in the ice cliff, causing small localised subaerial failures, and (ii) high magnitude events
487 which are associated with the propagation of suitably orientated surface crevasses and
488 outward bending of the ice cliff over the undercut, leading to collapse of the entire column.
489 Through analysis of the calving front before each event occurred, and based on the size of
490 each event overall, the type of calving failure observed in both July 2019 and 2021 was most
491 similar to mode (ii).

492 Before the July 2019 event, as well as the first event in July 2021, several large,
493 suitably orientated crevasses were observed at the ice surface, in the same region where these
494 large calving events later occurred (Fig. 6). Importantly, many of these crevasses were also
495 closely aligned to the precise failure surface of these events, and as a result we propose that
496 the undercutting of the terminus via notch development increased the force imbalances acting
497 on the terminal face, leading to a corresponding increase in the stresses acting on the ice
498 surface, which promoted fracture propagation until full failure occurred (Benn and others,
499 2007; 2017).

500 For the second event in 2021, although suitably orientated crevasses were again
501 observed (Fig. 6c), these were not as extensive as for the other two events. In this case, we
502 suggest that a combination of crevasse propagation, as well as the stress imbalance resulting
503 from the loss of a large volume of ice <24 hours prior were the likely drivers for this event.
504 As such, despite a lack of continuous observations, we believe calving occurred in a single,
505 large event on each occasion, rather than being made up of several smaller calving events
506 which occurred in quick succession.

507 Furthermore, based on the analyses presented in the study, we suggest these large
508 calving events were also likely responsible for the localised increases in velocity that were
509 observed in this region in both 2019 and 2021, particularly in the days that followed each
510 individual event (Figs. 5, S8 & S9). Previous work at several tidewater glaciers, e.g., in
511 Alaska and Greenland, has demonstrated that the balance of glacier stresses which control the
512 flow of calving glaciers are highly sensitive to any change in the position or thickness of the
513 calving front (Meier and Post, 1987; Howat and others, 2007; Nick and others, 2009). More
514 specifically, any sudden changes in the position of the calving front, whether glacier-wide or

515 localised (i.e., from a large calving event) will cause a reduction in the resistive stresses due
 516 to the sudden loss of a large volume of ice (Meier and Post, 1987; Joughin and others, 2008a;
 517 Howat and others, 2010; Murray and others, 2015). In response, the glacier speeds up and
 518 draws-down ice from higher elevations to provide the additional resistive stresses that are
 519 necessary to restore the stress balance (Howat and others, 2005; Pfeffer, 2007; Joughin and
 520 others, 2008a). As a result, brief periods of calving activity and retreat, lasting days or less,
 521 can result in an acceleration of ice flow that is sustained over a much longer period as the
 522 glacier evolves following the perturbation at the front (Joughin and others, 2008b; Howat and
 523 others, 2010; Murray and others, 2015).



524

525 **Fig. 6.** Orthomosaics from (a) 5 July 2019, (b) 4 July 2021 and (c) 6 July 2021, illustrating
 526 the presence of suitably orientated crevasses at the ice surface in the same region where the
 527 large calving events described in-text later occurred. Dashed red lines in each panel highlight
 528 the area of ice that calved in each event. Note how these lines closely correspond to the
 529 location and orientation of the crevasses at the ice surface, indicating that calving occurred
 530 along these lines of weakness. Location of (a) is given in Fig. 3a, whilst (b) & (c) are shown
 531 in Fig. 3b. Background in each panel is the orthomosaic for the respective day.

532 Although such a dynamic response has yet to be observed at a lake-terminating glacier
 533 in nature, and while we recognise there are notable differences between the processes
 534 occurring at large tidewater glaciers to those potentially underway here, based on the data
 535 presented in this study (Figs. 5, S8 & S9) we suggest that a similar set of processes may be
 536 occurring at Fjallsjökull, albeit at a smaller scale. Indeed, localised speed-ups are clearly
 537 observed in our velocity data, and as a result we suggest the following sequence of events

538 likely occurred in July 2021 (a similar sequence of events also occurred in this region in July
539 2019, but over a slightly shorter timescale):

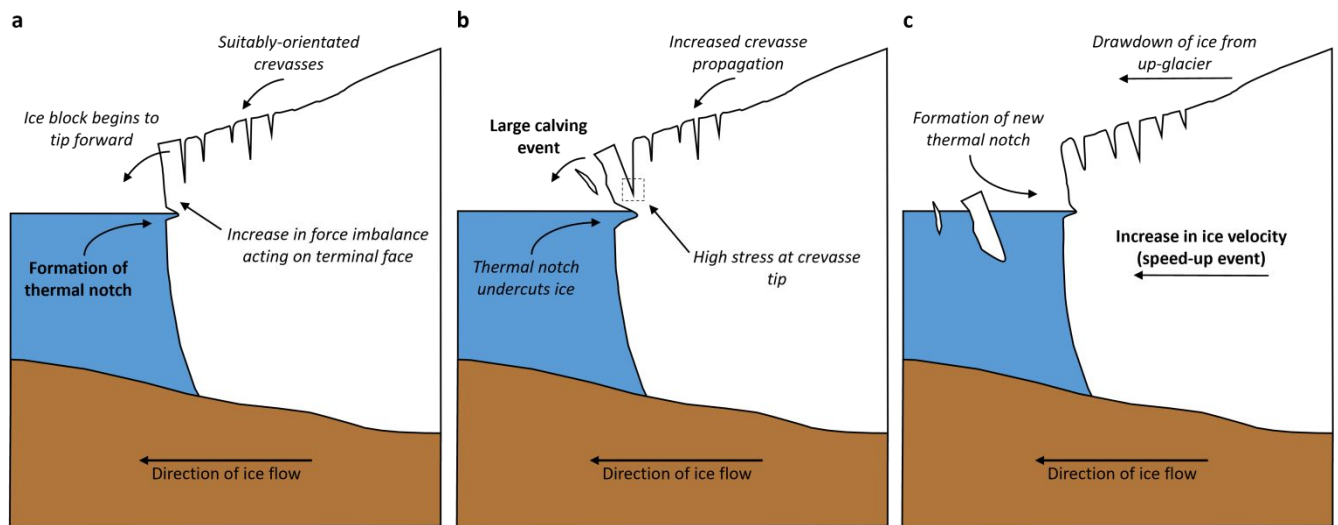
- 540 **(i)** The first calving event occurred between the 4 and 6 July, causing a reduction in the
541 resistive stresses and leading to locally high velocities ($\sim 0.72 \text{ m d}^{-1}$) in the region
542 immediately behind the new position of the calving front, but with little change in
543 velocity observed elsewhere.
544
- 545 **(ii)** The second large calving event occurred over the following 24 hours, causing this
546 region of locally high velocities to not only increase in areal extent, but to also increase
547 in magnitude (to $\sim 0.84 \text{ m d}^{-1}$). Consequently, it now extended some $\sim 400 \text{ m}$ back from
548 the calving front (encompassing much of the lower study region as a result), as well as
549 northwards, joining with the large region of high velocities in the upper portion of the
550 study area. Such a change likely reflects the speed-up and drawdown of ice from further
551 up-glacier in an attempt to restore the stress balance, following the sudden loss of a
552 large volume of ice in a relatively short period of time.
553
- 554 **(iii)** Over the following 48-hour period (7-9 July), although there was very little change in
555 the overall extent of this region of elevated velocities, a further increase in peak
556 velocity was observed during this time (to $\sim 0.94 \text{ m d}^{-1}$), indicating how ice acceleration
557 following calving failure can be sustained for several days after the initial event has
558 taken place.
559
- 560 **(iv)** It was only by the 11 July that velocities in this region had once again returned to their
561 pre-speed-up magnitude and extent, \sim five days after the initial calving event had
562 occurred.

563 Such short-term increases in velocity, occurring over relatively large areas of the
564 glacier in response to what were three large, but fundamentally localised, calving events,
565 highlights the importance of thermal notch erosion as a key control on both calving losses
566 (e.g., Röhl 2006; Minowa and others, 2017; Mallalieu and others, 2020) and localised ice
567 dynamics. These processes, and the chronology by which they occur at Fjallsjökull, are
568 summarised in Fig. 7.

569 It is possible that part of the velocity increase observed in both years may have been a
570 result of the glacier margin “resettling” and rotating forward in response to the new stress
571 regime post-calving (e.g., Benn and others, 2017), rather than being entirely related to ice
572 motion as described above. However, while these processes likely contributed to the observed
573 speed-ups, we do not believe they were the primary cause. This is for two reasons: (i) Our
574 time series of UAV-SfM orthomosaics and terrestrial imagery (Figs. S6, S7) provide no clear
575 evidence of the calving face rotating outwards in the days following calving, and (ii) if the
576 speed-up events were solely a result of this “resettling”, then the velocity increase that we
577 observed would have been limited to the area immediately behind the calving front, rather
578 than extending several hundred metres back from the terminus like is observed in our data.
579 As such, although these calving processes are important, they were unlikely to be the primary
580 driver of the observed speed-up events.

581 It is also important to note that due to the daily separation of our UAV surveys, we cannot
582 state with complete certainty whether these speed-ups occurred in direct response to the large
583 calving events. Instead, there is the potential that these calving events may have occurred as a
584 result of an increase in surface velocity. For completeness, therefore, we discuss three other

585 possible mechanisms for the observed speed-ups and explain why they can be discounted
 586 based on our observations.



587

588 **Fig. 7.** Summary schematic illustrating how (a) thermal notch erosion, (b) large calving
 589 events and (c) short-term speed up events are related (given in bold lettering), and the
 590 chronology by which these processes occur at Fjallsjökull, based on the data presented in this
 591 study. See main text for more detail on each process.

592 Recent work has shown that periods of relatively high air temperatures can cause
 593 calving glaciers to undergo short-term increases in velocity, due to peaks in subglacial water
 594 pressure (e.g., Sugiyama and others, 2011; Doyle and others, 2018; Jouvet and others, 2018).
 595 However, we find it unlikely that increased air temperatures were the primary driver behind
 596 the observed speed-ups, for four reasons.

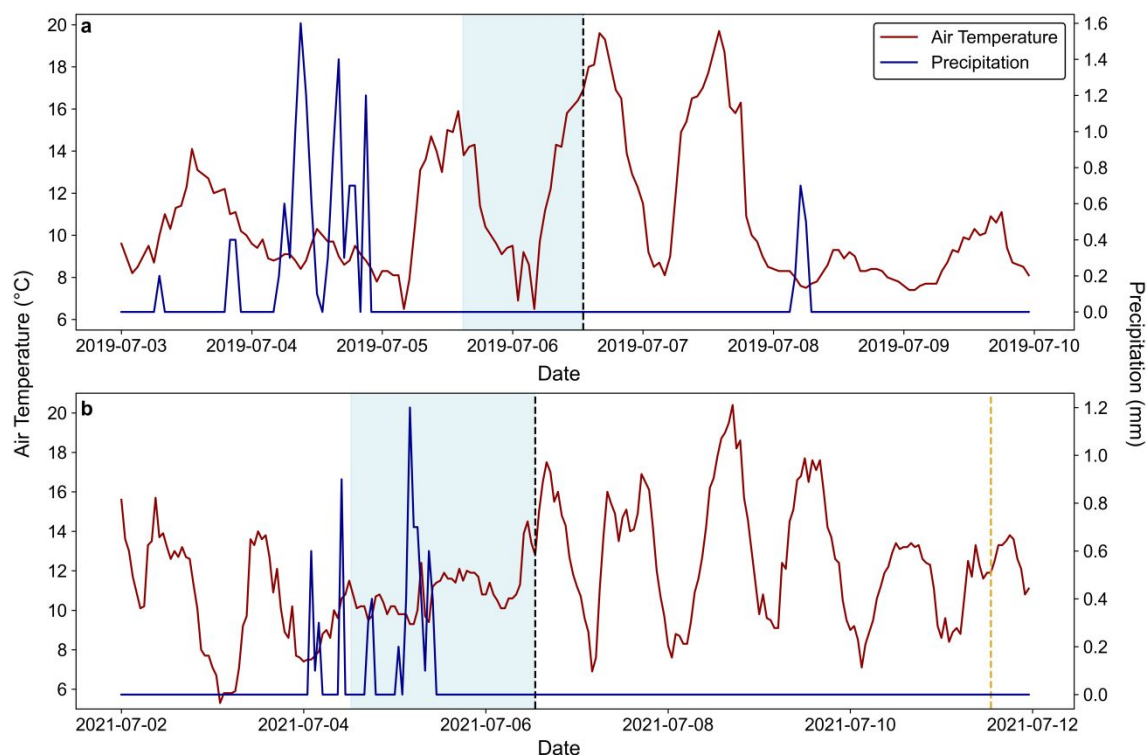
597 Firstly, and perhaps most significantly, both speed-up events were initially only
 598 constrained to a small region in the immediate vicinity of the calving front (Fig. 4). If air
 599 temperatures were the primary forcing mechanism, then we would expect this initial increase
 600 in velocity to occur over a much larger region of the glacier than is observed in our data (e.g.,
 601 Figs. 5, S8 & S9). Secondly, air temperatures were relatively low (Fig. 8) in the days
 602 preceding either of the speed-up events (average of $\sim 10.6^{\circ}\text{C}$), and, therefore, were unlikely to
 603 be sufficient to trigger the initial speed-up that was observed in both years.

604 Third, peak temperatures were only reached after the speed-up events had already
 605 begun, and while these high temperatures may have contributed to the duration of these
 606 events (particularly in 2021), as well as the overall magnitude of the velocity peaks observed
 607 in both years, their influence as a forcing mechanism is clearly limited as a result. Fourth, any
 608 increase in subglacial meltwater (from increased air temperatures) would need to leave the
 609 glacier front via a suitable discharge outlet (e.g., a meltwater plume), yet no obvious outlet or
 610 plume were observed in this region of the glacier in either year. As a result, we are confident
 611 that increased air temperatures, and concurrent peaks in subglacial discharge, can be ruled out
 612 as the primary driver of these events.

613 It has been demonstrated in several previous studies how intense periods of
 614 precipitation, totalling 10s mm in <24 hours, can cause calving glaciers to undergo rapid, but
 615 short-term (<24 -48-hour) increases in velocity (e.g., Sugiyama and others, 2015; How and

616 others, 2017). However, no precipitation fell in the 24-hours prior to the onset of the 2019
 617 event (Fig. 8a), and although some precipitation did fall prior to the 2021 event, this only
 618 totalled ~4.7 mm (Fig. 8b), which is unlikely to have been sufficient to trigger the initial
 619 speed-up that occurred in this year. As a result, we believe intense periods of precipitation
 620 can also be disregarded as a potential forcing mechanism.

621 Similarly, variations in the level of the proglacial water body can also impact glacier
 622 velocity over short timescales (e.g., Kirkbride and Warren, 1997; Dykes and others, 2011).
 623 However, our field observations (Figs. S6, S7) indicate that the level of Fjallsárlón changed
 624 very little across either study period, particularly before the onset of each speed-up event,
 625 suggesting that variations in lake level were also unlikely to be the primary cause.



626

627 **Fig. 8.** Hourly air temperature and precipitation data for (a) July 2019 and (b) July 2021.
 628 Legend in (a) is shared between both plots. Vertical dashed black lines indicate the onset of
 629 the speed-up events in both years, based on our UAV-SfM data, whilst the blue shaded
 630 regions mark the period in which the large calving events are known to have occurred.
 631 Vertical dashed gold line in (b) indicates the end of the speed-up event in 2021, based on our
 632 UAV-SfM data. Data obtained by the Icelandic Met Office from their weather station at
 633 Kvisker (63°58'N, 16°26'W, ~30 m a.s.l.), located ~5 km to the south of Fjallsjökull.

634 In contrast, because these large calving events were observed in the same region of the
 635 glacier across both years, and because the resultant speed-ups were only limited initially to
 636 the area immediately surrounding where these individual events occurred, suggests that these
 637 large calving events were the forcing mechanism, providing new insights into the dynamic
 638 behaviour of the glacier. To the best of our knowledge, we are the first study to demonstrate
 639 how these large calving events, occurring as a direct result of thermal notches at the
 640 waterline, can drive short-term increases in velocity at a lake-terminating glacier.

641 5.3. Wider Relevance and Future Outlook

642 It was previously suggested by Dell and others (2019) that calving at Fjallsjökull likely
643 occurs via a combination of buoyant forces acting on the terminus, force imbalances at
644 terminal ice cliffs and subaqueous melting, although they could not provide direct evidence
645 for any of these processes occurring. However, our field observations from both July 2019
646 and July 2021 provide direct evidence that subaqueous melting is occurring at the terminus of
647 Fjallsjökull, due to the presence of extensive thermal erosion notches at the waterline. Indeed,
648 we demonstrate how these notches can form and grow relatively rapidly at the waterline,
649 following calving. Furthermore, our data also indicate that these notches are the primary
650 driver of large calving events in this region, based not only on the size of the observed events,
651 but also from the evidence of extensive lines of weakness at the ice surface before these
652 events occurred. Finally, and perhaps most significantly, we have shown that these large
653 calving events can drive short-term increases in velocity, which are sustained for several days
654 and occur over a much larger area of the glacier than was originally impacted by the initial
655 event.

656 Our findings are likely to be important for other lake-terminating glaciers both in
657 Iceland, and elsewhere, where extensive thermal notches have been observed previously (e.g.,
658 Dykes and others, 2011; Minowa and others, 2017; Mallalieu and others, 2020). In Iceland,
659 for example, observations made by the authors over recent years have revealed the presence
660 of extensive waterline notches at several of the other southern outlets of Vatnajökull,
661 including Svínafellsjökull to the west and Briedamerkurjökull and Fláajökull to the east,
662 suggesting that the processes observed at Fjallsjökull in this study may also be occurring at
663 these glaciers. Likewise, for those regions where thermal notches are already known to exert
664 a key control on calving losses, such as in Patagonia and west Greenland (e.g., Minowa and
665 others, 2017; Mallalieu and others, 2020), there is the strong possibility that large calving
666 events may also result in short-term increases in ice velocity, underlining the need for further
667 research in these environments.

668 Furthermore, our findings may also be applicable to several tidewater glaciers, for
669 example in Svalbard, where calving, and large calving events in particular, are also known to
670 be driven by extensive notch erosion at the waterline (e.g., Pętllicki and others, 2015; How
671 and others, 2019). Yet despite extensive thermal notches being observed in these studies, and
672 that these notches drive calving behaviour in these settings, none were able to observe the
673 resultant short-term increases in velocity that we do here. Although this could be due to
674 several different factors, we believe a combination of the specific methodology chosen by
675 these studies, as well as how these studies have then employed these methods, to be the most
676 important.

677 For example, time-lapse photography has been employed in several previous studies to
678 acquire a continuous record of calving in both freshwater and tidewater environments (e.g.,
679 Medrzycka and others, 2015; How and others, 2019; Mallalieu and others, 2020), however,
680 the specific camera set-up used in these studies meant that any localised speed-ups which
681 may have occurred in response to calving were not quantified. Similarly, while methods such
682 as satellite remote sensing have also been used to investigate the role of melt undercutting on
683 calving rates (e.g., Luckman and others, 2015), the relatively coarse spatial and temporal
684 resolution of this imagery means it can be difficult to monitor processes occurring over fine
685 spatial and temporal scales (Pętllicki and others, 2015; Mallalieu and others, 2017; Jouvét and
686 others, 2018), such as the localised speed-up events observed here.

687 In contrast, this study has illustrated how UAV-SfM can be an effective and highly
688 suitable tool for the capture and monitoring of these speed-up events, due to the high spatial
689 and temporal resolution of the sensor. In particular, the “on demand” deployment of the UAV
690 system meant that we were able to undertake surveys almost every day (weather permitting),
691 allowing variations in ice velocity to be investigated at a temporal resolution that would be
692 nearly impossible to obtain using more traditional techniques. Furthermore, although it was
693 not specifically done here, it would have also been possible to undertake multiple surveys
694 each day, which may have provided important additional insights into these events.

695 However, despite its ability to accurately capture and monitor these speed-up events,
696 UAV-SfM importantly has two limitations when deployed for this purpose: (i) direct
697 measurements of notch morphology can often be difficult to obtain, and (ii) it does not
698 provide a continuous record of change. For example, while the method can be used to provide
699 an estimation of the total amount of ice that calved between successive surveys (like done
700 here), often the temporal resolution is still too coarse to be able to determine when exactly
701 these calving events occurred, and consequently, whether these calving events do drive short-
702 term increases in velocity. Yet, while we are confident that the speed-ups observed here did
703 occur as a direct result of calving, additional work is clearly required.

704 As a result, we suggest future studies:

- 705 (i) Utilise a combination of both UAV-SfM surveys and terrestrial time-lapse photography
706 in order to address the limitations described above, as well as to ensure the accurate
707 determination of glacier velocity at high spatial and temporal scales.
- 708 (ii) Obtain direct measurements of surface water temperature, as well as how the level of
709 the waterbody fluctuates (e.g., Röhl, 2006; Minowa and others, 2017), in order to
710 calculate the notch erosion rate, and how this varies through time (due to the lack of
711 quantitative data relating to the thermal erosion process, e.g., Mallalieu and others,
712 2020).
- 713 (iii) Employ these methods across a larger number of glaciers in both freshwater and
714 tidewater settings in order to increase the number of detailed and high-resolution in-situ
715 field observations from these environments, the data of which may then be used to help
716 further constrain calving processes in glacier and ice sheet models (e.g., Benn and
717 others, 2017).

718 Ultimately, this would allow these processes, and in particular, these localised speed-up
719 events, to be investigated in extremely high detail across a range of glaciated regions,
720 providing valuable insights into the relative importance of these processes, not just for the
721 dynamic behaviour of these glaciers, but also their overall stability, both at present and in the
722 future.

723 6. CONCLUSION

724 In this study, we utilised repeat high-resolution UAV-SfM surveys, alongside terrestrial
725 photography acquired in-situ, to investigate the role of thermal notch erosion in forcing
726 localised calving failure and subsequent short-term increases in velocity at an actively calving
727 lake-terminating glacier in southeast Iceland. This data was acquired daily (where possible)
728 across one week in July 2019 and two weeks in July 2021 to provide insights into a suite of
729 processes that have been rarely studied. We show that extensive thermal notches are present

730 at the waterline in both years, and that the relative size of these features varies over time. We
731 also illustrate how new notches can form and grow relatively rapidly at the waterline
732 following calving (<24 hours), and although no direct measurements of notch erosion could
733 be made here, based on the size of these features, and how rapidly they formed, it is not
734 inconceivable that rates of $\sim 0.5 \text{ m d}^{-1}$ could be possible.

735 Importantly, we demonstrate that these notches are the primary driver of large calving
736 events in this region of the glacier, based not only on the size of the observed events (surface
737 area $>1000 \text{ m}^2$, $>150 \text{ m}$ wide), but also from the evidence of extensive lines of weakness at
738 the ice surface before these events occurred. Finally, and perhaps most significantly, we have
739 shown that these large calving events can drive short-term increases in velocity, which are
740 sustained for several days and occur over a much larger area of the glacier than was originally
741 impacted by the initial event. In 2019, velocities were $\sim 25\%$ faster than the average, peaking
742 ~ 24 hours after the initial calving event, before beginning to decrease. In 2021 velocities
743 were $\sim 30\%$ faster than the average, but due to the occurrence of two large calving events in
744 the space of two days, velocities did not peak until three days after the initial event.
745 Velocities only then returned to their pre-speed-up magnitude two days later.

746 To the best of our knowledge, we are the first study to demonstrate how these large
747 calving events, occurring as a direct result of thermal notches at the waterline, can drive
748 short-term increases in velocity at a lake-terminating glacier. Therefore, our findings present
749 an important and previously undocumented aspect of calving glacier behaviour, which has
750 the potential to occur in both freshwater and tidewater environments. However, due to a lack
751 of similar high-resolution field studies in these environments, the relative importance of these
752 processes remains unknown. As a result, we strongly suggest that future studies investigate
753 the importance of these processes across a larger number of calving glaciers in both
754 freshwater and tidewater settings, in order to better understand their dynamic behaviour and
755 overall stability, both at present and in the future.

756 **CONFLICT OF INTEREST STATEMENT**

757 The authors declare that the research was conducted in the absence of any commercial or
758 financial relationships that could be construed as a potential conflict of interest.

759 **DATA AVAILABILITY STATEMENT**

760 The datasets generated for this study can be found in the following repositories:
761 <https://doi.org/10.5281/zenodo.7105133> and <https://doi.org/10.5281/zenodo.7111111>.

762 **AUTHOR CONTRIBUTIONS**

763 NB and JH devised the study. NB undertook the fieldwork, processed and analysed the UAV
764 data and wrote the draft version of the manuscript. Both authors contributed to the writing
765 and editing of the final manuscript.

766 **SUPPLEMENTARY MATERIAL**

767 The supplementary material for this article can be found at: [LINK]

768 **ACKNOWLEDGEMENTS**

769 The authors acknowledge the comments of three anonymous reviewers which greatly
 770 improved the quality of the manuscript. NB wishes to thank David Sutherland and Chris
 771 Tomsett for their assistance across the two field campaigns, as well as the Vatnajökull
 772 National Park for providing a research permit to allow these campaigns to be undertaken. NB
 773 acknowledges funding from several sources: The July 2019 field campaign was funded by a
 774 Postgraduate Research Award from the Royal Geographical Society (with IBG), whilst the
 775 July 2021 field campaign was funded by a Dudley Stamp Memorial Award (part of the
 776 Postgraduate Research Awards) from the Royal Geographical Society (with IBG), and an
 777 expedition grant from The Mount Everest Foundation.

778 **REFERENCES**

- 779 Agisoft LLC (2021) Agisoft Metashape User Manual: Professional edition, Version 1.7. [online]. Agisoft LLC.
 780 Available from: <https://www.agisoft.com/downloads/user-manuals/> [Accessed: 23rd September 2021].
- 781 Bartholomaeus TC, Larsen CF and O'Neel S (2013) Does calving matter? Evidence for significant submarine melt.
 782 *Earth Planet. Sci. Lett.*, **380**, 21–30. (doi: 10.1016/j.epsl.2013.08.014)
- 783 Bash EA, Moorman BJ and Gunther A (2018) Detecting short-term surface melt on an Arctic Glacier using UAV
 784 surveys. *Remote Sens.*, **10**(10), 1–17. (doi: 10.3390/rs10101547)
- 785 Baurley, NR (2022) *Insights into the seasonal dynamics of the lake-terminating glacier Fjallsjökull, south-east
 786 Iceland, inferred using ultra-high resolution repeat UAV imagery*. PhD thesis, University of Southampton, UK.
 787 (doi: eprints.soton.ac.uk/471220/)
- 788 Baurley NR, Tomsett C and Hart JK (2022) Assessing UAV-based laser scanning for monitoring glacial processes
 789 and interactions at high spatial and temporal resolutions. *Front. Remote Sens.*, **3**, 1027065. (doi:
 790 10.3389/frsen.2022.1027065)
- 791 Baurley NR, Robson BA and Hart JK (2020) Long-term impact of the proglacial lake Jökulsárlón on the flow
 792 velocity and stability of Breiðamerkurjökull glacier, Iceland. *Earth Surf. Process. Landf.*, **45**(11), 2647–2663.
 793 (doi: 10.1002/esp.4920)
- 794 Benn DI and Åström JA (2018) Calving glaciers and ice shelves. *Adv. Phys-X*, **3**(1), 1513819. (doi:
 795 10.1080/23746149.2018.1513819)
- 796 Benn, DI and 7 others (2017) Melt-under-cutting and buoyancy driven calving from tidewater glaciers: new insights
 797 from discrete element and continuum model simulations. *J. Glaciol.*, **63**(240), 691–702. (doi:
 798 10.1017/jog.2017.41)
- 799 Benn DI, Warren CR and Mottram RH (2007) Calving processes and the dynamics of calving glaciers. *Earth-Sci.
 800 Rev.*, **82**(3–4), 143–179. (doi: 10.1016/j.earscirev.2007.02.002)
- 801 Carrivick JL, Tweed FS, Sutherland JL and Mallalieu J (2020) Toward numerical modelling of interactions between
 802 ice-marginal proglacial lakes and glaciers. *Front. Earth Sci.*, **8**, 577068. (doi: 10.3389/feart.2020.577068)
- 803 Chudley T, Christoffersen P, Doyle SH, Abellan A and Snooke N (2019) High accuracy UAV photogrammetry of
 804 ice sheet dynamics with no ground control. *Cryosphere*, **13**(3), 955–968. (doi: 10.5194/tc-13-955-2019)
- 805 Dell R, Carr R, Phillips E and Russell AJ (2019) Response of glacier flow and structure to proglacial lake
 806 development and climate at Fjallsjökull, south-east Iceland. *J. Glaciol.*, **65**(250), 321–336. (doi:
 807 10.1017/jog.2019.18)
- 808 Doyle, S and 7 others (2018) Physical conditions of fast glacier flow: 1. Measurements from boreholes drilled to the
 809 bed of store glacier, west Greenland. *J. Geophys. Res. Earth Surf.*, **123**, 324–348. (doi: 10.1002/2017JF004529)
- 810 Dykes RC, Brook MS, Robertson CM and Fuller IC (2011) Twenty-first century calving retreat of Tasman Glacier,
 811 Southern Alps, New Zealand. *Arct. Antarct. Alp. Res.*, **43**(1), 1–10. (doi: 10.1657/1938-4246-43.1.1)

- 812 Ely JC, Graham C, Barr ID, Rea BR, Spagnolo M and Evans J (2017) Using UAV acquired photography and
813 structure from motion techniques for studying glacier landforms: Application to the glacial flutes at
814 Isfallsglaciären. *Earth Surf. Process. Landf.*, **42**(6), 877–888. (doi: 10.1002/esp.4044)
- 815 Evans DJ and Twigg DR (2002) The active temperate glacial landsystem: A model based on Breiðamerkurjökull
816 and Fjallsjökull, Iceland. *Quat. Sci. Rev.*, **21**(20–22), 2143–2177. (doi: 10.1016/S0277-3791(02)00019-7)
- 817 Guðmundsson S, Björnsson H, Pálsson F, Magnússon E, Sæmundsson Þ and Jóhannesson T (2019) Terminus lakes
818 on the south side of Vatnajökull ice cap, SE-Iceland. *Jökull*, **69**, 1–34.
- 819 Hannesdóttir H, Björnsson H, Pálsson F, Aðalgeirsdóttir G and Guðmundsson S (2015) Changes in the southeast
820 Vatnajökull ice cap, Iceland, between ~1890 and 2010. *Cryosphere*, **9**(2), 565–585. (doi: 10.5194/tc-9-565-
821 2015)
- 822 Haresign E and Warren CR (2005) Melt rates at calving termini: A study at Glaciar Leon, Chilean Patagonia. *Geol.*
823 *Soc. Lond. Spec. Publ.*, **242**, 99–109. (doi: 10.1144/GSL.SP.2005.242.01.09)
- 824 Haug T, Kääb A and Skvarca P (2010) Monitoring ice shelf velocities from repeat MODIS and Landsat data-a
825 method study on the Larsen C ice shelf, Antarctic Peninsula, and 10 other ice shelves around
826 Antarctica. *Cryosphere*, **4**(2), 161–178. (doi: 10.5194/tc-4-161-2010)
- 827 Heid T and Kääb A (2012) Evaluation of existing image matching methods for deriving glacier surface
828 displacements globally from optical satellite imagery. *Remote Sens. Environ.*, **118**, 339–355. (doi:
829 10.1016/j.rse.2011.11.024)
- 830 Höhle J and Höhle M (2009) Accuracy assessment of digital elevation models by means of robust statistical
831 methods. *ISPRS J. Photogramm. Remote Sens.*, **64**(4), 398–406. (doi: 10.1016/j.isprsjprs.2009.02.003)
- 832 How, P and 8 others (2019) Calving controlled by melt-under-cutting: Detailed calving styles revealed through
833 time-lapse observations. *Ann. Glaciol.*, **60**(78), 20–31. (doi: 10.1017/aog.2018.28)
- 834 How, P and 9 others (2017) Rapidly changing subglacial hydrological pathways at a tidewater glacier revealed
835 through simultaneous observations of water pressure, supraglacial lakes, meltwater plumes and surface
836 velocities. *Cryosphere*, **11**(6), 2691–2710. (doi: 10.5194/tc-11-2691-2017)
- 837 Howat IM, Box JE, Ahn Y, Herrington A and McFadden EM (2010) Seasonal variability in the dynamics of
838 marine-terminating outlet glaciers in Greenland. *J. Glaciol.*, **56**(198), 601–613. (doi:
839 10.3189/002214310793146232)
- 840 Howat IM, Joughin I and Scambos TA (2007) Rapid changes in ice discharge from Greenland outlet
841 glaciers. *Science*, **315**(5818), 1559–1561. (doi: 10.1126/science.1138478)
- 842 Howat IM, Joughin I, Tulaczyk S and Gogineni S (2005) Rapid retreat and acceleration of Helheim Glacier, east
843 Greenland. *Geophys. Res. Lett.*, **32**, L22502. (doi:10.1029/2005gl024737)
- 844 Immerzeel, WW and 6 others (2014) High-resolution monitoring of Himalayan glacier dynamics using unmanned
845 aerial vehicles. *Remote Sens. Environ.*, **150**, 93–103. (doi: 10.1016/j.rse.2014.04.025)
- 846 Jenkins A (2011) Convection-driven melting near the grounding lines of ice shelves and tidewater glaciers. *J. Phys.*
847 *Oceanogr.*, **41**(12), 2279–2294. (doi: 10.1175/JPO-D-11-03.1)
- 848 Joughin, I and 8 others (2008a) Ice-front variation and tidewater behaviour on Helheim and Kangerdlugssuaq
849 Glaciers, Greenland. *J. Geophys. Res. Earth Surf.*, **113**(F1). (doi: 10.1029/2007JF000837)
- 850 Joughin, I and 7 others (2008b) Continued evolution of Jakobshavn Isbrae following its rapid speedup. *J. Geophys.*
851 *Res. Earth Surf.*, **113**(F4). (doi: 10.1029/2008JF001023)
- 852 Jouvét G, Weidmann Y, van Dongen E, Luethi M, Vieli A and Ryan J (2019) High-endurance UAV for monitoring
853 calving glaciers: Application to the Inglefield Bredning and Eqip Sermia, Greenland. *Front. Earth Sci.*, **7**, 206.
854 (doi: 10.3389/feart.2019.00206)
- 855 Jouvét, G and 6 others (2018) Short-lived ice speed-up and plume water flow captured by a VTOL UAV give
856 insights into subglacial hydrological system of Bowdoin Glacier. *Remote Sens. Environ.*, **217**, 389–399. (doi:
857 10.1016/j.rse.2018.08.027)

- 858 Jouvett, G and 7 others (2017) Initiation of a major calving event on the Bowdoin Glacier captured by UAV
859 photogrammetry. *Cryosphere*, **11**(2), 911–921. (doi: 10.5194/tc-11-911-2017)
- 860 Kirkbride M and Warren C (1997) Calving processes at a grounded ice cliff. *Ann. Glaciol.*, **24**, 116–121. (doi:
861 10.3189/S0260305500012039)
- 862 Lague D, Brodu N and Leroux J (2013) Accurate 3D comparison of complex topography with terrestrial laser
863 scanner: Application to the Rangitikei canyon (NZ). *ISPRS J. Photogramm. Remote Sens.*, **82**, 10–26. (doi:
864 10.1016/j.isprsjprs.2013.04.009)
- 865 Luckman, A and 5 others (2015) Calving rates at tidewater glaciers vary strongly with ocean temperature. *Nat.*
866 *Commun.*, **6**, 8566. (doi: 10.1038/ncomms9566)
- 867 Magnússon E, Pálsson F, Björnsson H and Guðmundsson S (2012) Removing the ice cap of Öräfajökull central
868 volcano, SE Iceland: Mapping and interpretation of bedrock topography, ice volumes, subglacial troughs and
869 implications for hazards assessments. *Jökull*, **62**, 131–150.
- 870 Mallalieu J, Carrivick JL, Quincey DJ and Smith MW (2020). Calving seasonality associated with
871 melt-undercutting and lake ice cover. *Geophys. Res. Lett.*, **47**, e2019GL086561. (doi: 10.1029/2019GL086561)
- 872 Mallalieu J, Carrivick JL, Quincey DJ, Smith MW and James WHM (2017) An integrated structure-from-motion
873 and time-lapse technique for quantifying ice-margin dynamics. *J. Glaciol.*, **63**(242), 937–949. (doi:
874 10.1017/jog.2017.48)
- 875 Medrzycka D, Benn DI, Box JE, Copland L and Balog J (2016) Calving behavior at Rink Isbræ, West Greenland,
876 from timelapse photos. *Arct. Antarct. Alp. Res.*, **48**(2), 263–277. (doi: 10.1657/AAAR0015-059)
- 877 Meier MF and Post (1987) Fast tidewater glaciers. *J. Geophys. Res. Solid Earth*, **92**(B9), .9051–9058. (doi:
878 10.1029/JB092iB09p09051)
- 879 Minowa M, Sugiyama S, Sakakibara D and Skvarca P (2017) Seasonal variations in ice-front position controlled by
880 frontal ablation at Glaciar Perito Moreno, the Southern Patagonia Icefield. *Front. Earth Sci.*, **5**, 1. (doi:
881 10.3389/feart.2017.00001)
- 882 Murray, T and 9 others (2015) Dynamics of glacier calving at the ungrounded margin of Helheim Glacier, southeast
883 Greenland. *J. Geophys. Res. Earth Surf.*, **120**, 964–982. (doi: 10.1002/2015jf003531)
- 884 Nick FM, Vieli A, Howat IM and Joughin I (2009) Large-scale changes in Greenland outlet glacier dynamics
885 triggered at the terminus. *Nat. Geosci.*, **2**(2), 110–114. (doi: 10.1038/ngeo394)
- 886 O’Leary M and Christoffersen P (2013) Calving on tidewater glaciers amplified by submarine frontal melting.
887 *Cryosphere*, **7**(1), 119–128. (doi: 10.5194/tc-7-119-2013)
- 888 Pętliski M, Ciepły M, Jania JA, Promińska A and Kinnard C (2015) Calving of a tidewater glacier driven by
889 melting at the waterline. *J. Glaciol.*, **61**(229), 851–863. (doi: 10.3189/2015JoG15J062)
- 890 Pfeffer, WT (2007) A simple mechanism for irreversible tidewater glacier retreat. *J. Geophys. Res. Earth Surf.*,
891 **112**(F3). (doi: 10.1029/2006JF000590)
- 892 Purdie H, Bealing P, Tidey E, Gomez C and Harrison J (2016) Bathymetric evolution of Tasman Glacier terminal
893 lake, New Zealand, as determined by remote surveying techniques. *Glob. Planet. Change*, **147**, 1–11. (doi:
894 10.1016/j.gloplacha.2016.10.010)
- 895 Rignot E, Fenty I, Xu Y, Cai C and Kemp C (2015) Undercutting of marine-terminating glaciers in West
896 Greenland. *Geophys. Res. Lett.*, **42**(14), 5909–5917. (doi: 10.1002/2015GL064236)
- 897 Robson BA, Nuth C, Nielsen PR, Girod, L, Hendrickx M and Dahl SO (2018) Spatial variability in patterns of
898 glacier change across the Manaslu Range, Central Himalaya. *Front. Earth Sci.*, **6**, 12. (doi:
899 10.3389/feart.2018.00012)
- 900 Röhl K (2006) Thermo-erosional notch development at fresh-water-calving Tasman Glacier, New Zealand. *J.*
901 *Glaciol.*, **52**, 203–213. (doi: 10.3189/172756506781828773)
- 902 Rossini, M and 7 others (2018) Rapid melting dynamics of an alpine glacier with repeated UAV
903 photogrammetry. *Geomorphology*, **304**, 159–172. (doi: 10.1016/j.geomorph.2017.12.039)

- 904 Ryan, JC and 7 others (2015) UAV photogrammetry and structure from motion to assess calving dynamics at Store
905 Glacier, a large outlet draining the Greenland ice sheet. *Cryosphere*, **9**, 1–11. (doi: 10.5194/tc-9-1-2015)
- 906 Schild, KM and 9 others (2018) Glacier calving rates due to subglacial discharge, fjord circulation, and free
907 convection. *J. Geophys. Res. Earth Surf.*, **123**, 2189–2204. (doi: 10.1029/2017JF004520)
- 908 Sugiyama S, Sakakibara D, Tsutaki S, Maruyama M and Sawagaki T (2015) Glacier dynamics near the calving
909 front of Bowdoin Glacier, northwestern Greenland. *J. Glaciol.*, **61**(226), 223–232. (doi:
910 10.3189/2015JoG14J127)
- 911 Sugiyama, S and 7 others (2011) Ice speed of a calving glacier modulated by small fluctuations in basal water
912 pressure. *Nat. Geosci.*, **4**(9), 597–600. (doi: 10.1038/ngeo1218)
- 913 Tomsett C and Leyland J (2021) Development and Testing of a UAV Laser Scanner and Multispectral Camera
914 System for Eco-Geomorphic Applications. *Sensors*, **21**(22), 7719. (doi: 10.3390/s21227719)
- 915 Truffer M and Motyka RJ (2016) Where glaciers meet water: Subaqueous melt and its relevance to glaciers in
916 various settings. *Rev. Geophys.*, **54**(1), 220–239. (doi: 10.1002/2015RG000494)
- 917 Westoby MJ, Brasington J, Glasser NF, Hambrey MJ and Reynolds JM (2012) ‘Structure-from-Motion’
918 photogrammetry: A low-cost, effective tool for geoscience applications. *Geomorphology*, **179**, 300–314. (doi:
919 10.1016/j.geomorph.2012.08.021)
- 920 Whitehead K, Moorman BJ and Hugenholtz CH (2013) Brief Communication: Low-cost, on-demand aerial
921 photogrammetry for glaciological measurement. *Cryosphere*, **7**(6), 1879–1884. (doi: 10.5194/tc-7-1879-2013)
- 922 Wigmore O and Mark BG (2017) Monitoring tropical debris-covered glacier dynamics from high-resolution
923 unmanned aerial vehicle photogrammetry, Cordillera Blanca, Peru. *Cryosphere*, **11**, 2463–2480. (doi:
924 10.5194/tc-11-2463-2017)
- 925 Xue Y, Jing Z, Kang S, He X and Li C (2021) Combining UAV and Landsat data to assess glacier changes on the
926 central Tibetan Plateau. *J. Glaciol.*, **67**(265), 1–13. (doi: 10.1017/jog.2021.37)
- 927 Yang, W and 8 others (2020) Seasonal Dynamics of a Temperate Tibetan Glacier Revealed by High-Resolution
928 UAV Photogrammetry and In Situ Measurements. *Remote Sens.*, **12**(15), 2389. (doi: 10.3390/rs12152389)